energies

MDPI

Article

A Time-Efficient and Accurate Open Circuit Voltage Estimation Method for Lithium-Ion Batteries

Yingjie Chen *, Geng Yang, Xu Liu and Zhichao He

Department of Automation, Tsinghua University, Beijing 100084, China; yanggeng@tsinghua.edu.cn (G.Y.); liuxu16@mails.tsinghua.edu.cn (X.L.); hzc_thu@163.com (Z.H.)

* Correspondence: chenyingjie0323@126.com

Received: 9 March 2019; Accepted: 8 May 2019; Published: 12 May 2019

Abstract: The open circuit voltage (OCV) of lithium-ion batteries is widely used in battery modeling, state estimation, and management. However, OCV is a function of state of charge (SOC) and battery temperature (T_{bat}) and is very hard to estimate in terms of time efficiency and accuracy. This is because two problems arise in normal operations: (1) T_{bat} changes with the current (I), which makes it very hard to obtain the data required to estimate OCV—terminal voltage (U) data of different I under the same T_{bat}; (2) the difference between U and OCV is a complex nonlinear function of I and is very difficult to accurately calculate. Therefore, existing methods have to design special experiments to avoid these problems, which are very time consuming. The proposed method consists of a designed test and a data processing algorithm. The test is mainly constant current tests (CCTs) of large I, which is time-efficient in obtaining data. The algorithm solves the two problems and estimates OCV accurately using the test data. Experimental results and analyses showed that experimental time was reduced and estimation accuracy was adequate.

Keywords: lithium-ion battery; open circuit voltage estimation; state of charge; battery temperature

1. Introduction

The open circuit voltage (OCV) of a lithium-ion battery is the terminal voltage (U) when the internal physical and chemical processes of the battery are steady [1]. OCV is widely used for battery modeling [2,3], state estimation [4,5], and management [6], etc., and is in need of estimation. An applicable OCV estimation method at a product level requires a short experimental time and adequate accuracy.

The principle of OCV estimation methods can be explained by the equivalent circuit models (ECMs) of the battery. The most widely used ECM is shown in Figure 1 [2], where U is terminal voltage, I is working current (this study defines discharge as the positive direction), Z is equivalent impedance, and ΔU is the voltage drop across Z. It is worth noting that Z represents the internal multidynamics of the battery, such as ohm polarization, electrochemical polarization, and concentration polarization [1]. The typical time ranges of these internal dynamics can be from microseconds to as long as hours [7], which means long time rests are required before these dynamics become steady states. Existing studies have shown that OCV is mainly a nonlinear function of state of charge (SOC) and battery temperature (T_{bat}) [8], while Z and therefore ΔU are nonlinear functions of SOC, I, and T_{bat} [9]. This study defines the working point of a battery as {SOC, I, T_{bat}}. Therefore, OCV, ΔU, and U are restricted as follows at each working point according to the ECM of Figure 1:

$$\mathrm{OCV}(\mathrm{SOC}, T_{bat}) - \Delta U(\mathrm{SOC}, I, T_{bat}) = U(\mathrm{SOC}, I, T_{bat}), \quad (1)$$

where U and I can be measured easily and accurately with test equipment. T_{bat} is a field-distributed parameter, but can be treated as a lumped parameter in the case of OCV estimation [10]. Further, T_{bat} can be measured with a thermocouple for simplification [10]. SOC can be calculated with Equation (2) [11]:

$$\mathrm{SOC}(t) = \mathrm{SOC}(t_0) - \frac{1}{C_{\mathrm{nom}}} \int_{t_0}^{t} I(t)\mathrm{d}t, \tag{2}$$

where C_{nom} is the nominal capacity of the battery, t is the operation time, and t_0 is the start time of the operation. It is generally considered that SOC equals one when the battery is fully charged. To sum up, U, I, SOC, and T_{bat} in Equation (1) can be measured or calculated, while both OCV and ΔU are unknown variables.

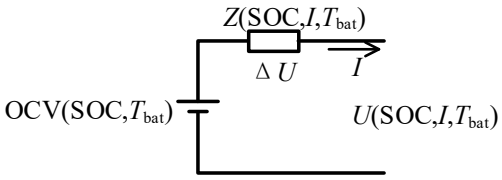

Figure 1. An equivalent circuit model (ECM) of batteries.

An estimation of OCV can be done through applying multiple current excitations to the model and analyzing the corresponding U variations. However, there are two difficulties in estimating OCV, especially under large-current conditions, which is a common working state in many applications. The first one is that the parameters are functions of SOC and T_{bat}, and therefore estimation needs U data of different I under the same {SOC,T_{bat}}. However, T_{bat} is affected by I and changes drastically under large-current conditions [7,12], as shown in Figure 2. This means discharging/charging the battery with different I to the same SOC results in different T_{bat}, which makes it almost impossible to obtain U data of different I under the same {SOC,T_{bat}} directly through experiments. The second one is that ΔU and Z are time-varying and nonlinear functions of I, and the forms of these functions are very complicated due to the complicated dynamics inside the battery [1], which makes it very difficult to determine the ΔU–I function accurately under large-current conditions. These two problems are referred to as T_{bat} changing with I and complex ΔU–I nonlinearity problems hereinafter and must be solved by an effective and, more importantly, engineering-oriented parameter estimation method.

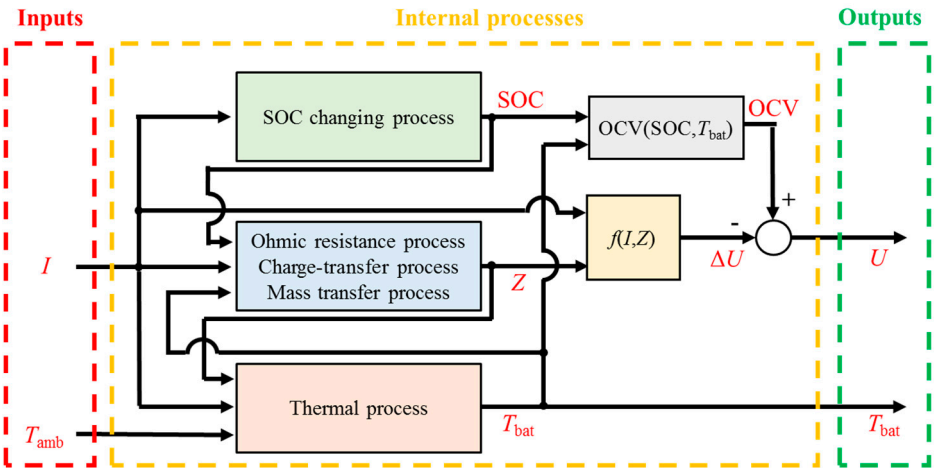

Figure 2. Inputs, outputs, and main internal processes of the battery (T_{amb}: ambient temperature).

The existing methods can be divided into two groups, voltage relaxation (VR) methods [13–17] and constant current (CC) methods [18–20], according to the form of the test signals.

The long time rest (LTR) method [13] is the most accurate VR method. At a certain {SOC,T_{bat}}, the LTR method rests the battery for about 20 h to stabilize the battery internal dynamics. During the rest, ΔU converges to zero, SOC remains the same, and T_{bat} converges to T_{amb} (ambient temperature), so both T_{bat} changing with I and the complex ΔU–I nonlinearity problems can be avoided through the test design. Therefore, the LTR method can directly take U at the end of the rest as the OCV at the working point {SOC,T_{bat}}. The LTR method repeatedly rests the battery at other working points to perform corresponding OCV estimations. The estimation results are so accurate that they are often treated as the OCV true value. However, this method is very time consuming, since long time rest tests must be conducted at extensive working points.

The hybrid pulse power characterization (HPPC) [14,15] method is the most widely used VR method. The only difference between HPPC and LTR is that the rest time is shortened to one hour. The HPPC method is accurate, since ΔU gradually converges to zero during rest and a one-hour rest can achieve adequate accuracy in most engineering applications. HPPC is far less time consuming than the LTR method and can fit the experimental time requirements for applications such as SOC estimation, which only requires OCV estimation results at 10–20 SOC points under each T_{bat}. However, in applications such as battery aging evaluations, it is necessary to differentiate the OCV–SOC curve for incremental capacity analysis (ICA) to expose the battery's internal changes [16], so it is necessary to estimate OCV at over 1000 SOC points under each T_{bat}. The HPPC method is still too time consuming for such applications.

Terminal voltage prediction (TVP) methods [17] are the least time consuming VR methods. These methods model the U–t (time) relationship during battery rest and can estimate the OCV under a certain {SOC,T_{bat}} with only a 20-min rest. These methods are still accurate enough as long as the U–t relationship is accurately modeled. Besides, these methods are less time consuming than the HPPC method due to the rest time being further shortened and can fit SOC estimation applications quite well. However, TVP methods still cannot meet the experimental time requirements of ICA.

The small-current approximation (SCA) [20] method is a typical CC method. The SCA method conducts a constant current test (CCT) with small I (about 1/25 C, where C is battery C rate) under a constant T_{amb}. The SCA method neglects ΔU and assumes $T_{bat} = T_{amb}$ in a small-current CCT, and therefore both T_{bat} changing with I and complex ΔU–I nonlinearity problems are neglected. The SCA method can directly take U in the CCT as the OCV. By conducting small-current CCTs under other T_{amb}, the SCA method can estimate OCV(SOC,T_{bat}). The SCA method can obtain OCV estimation results at thousands of SOC points or more through just one CCT due to the high sampling frequency of the test equipment. Moreover, the changes in T_{bat} are not obvious in a small-current CCT, so it is reasonable to assume $T_{bat} = T_{amb}$. However, neglecting ΔU causes significant errors. In addition, this is still time consuming, since each small-current CCT takes a long time (about 30 h).

Another CC method, the terminal voltage average (TVA) method [18,19], attempts to improve the accuracy of the SCA method. The TVA method conducts two small-current (also about 1/25 C) CCTs with equal current amplitude but in opposite directions under each T_{amb}. By assuming the ΔU–I relation is linear near $I = 0$, the TVA method calculates OCV as the average U of the two CCTs. This method is more accurate than SCA since it considers the ΔU–I relation approximately. However, the TVA method is still not very accurate (see Section 4) and consumes about twice the experimental time (about 55 h under each T_{amb}) in contrast to the SCA method due to the need for two CCTs.

To sum up, a battery usually works under large-current conditions in actual applications, which accordingly causes T_{bat} changing with I and complex ΔU–I nonlinearity problems in OCV estimation. Existing OCV estimation methods need to design special experiments to avoid these two problems. VR methods conduct rest experiments and can provide accurate estimation results. Some of the VR methods (HPPC and TVP) can adequately meet the experimental time requirement for applications such as SOC estimation, which only requires OCV estimation results at 10–20 SOC points under each T_{bat}. However, VR methods are too time consuming for applications such as ICA, which requires OCV estimation results at over 1000 SOC points under each T_{bat}. Differently,

CC methods conduct small-current CCTs and can estimate OCV at thousands of SOC points or more with much less experimental time. However, CC methods are not very accurate and are still time consuming.

This paper solves T_{bat} changing with I and complex ΔU–I nonlinearity problems and proposes an OCV(SOC,T_{bat}) estimation method that is time-efficient and adequately accurate in engineering applications. The method contains a designed test and a data processing algorithm. Large-current CCTs instead of small-current CCTs are conducted to be time-efficient in collecting necessary data. The algorithm is based on a battery electrochemical mechanism, can solve T_{bat} changing with I and complex ΔU–I nonlinearity problems, and can therefore estimate OCV(SOC,T_{bat}) accurately. The proposed method was verified via experiments and compared with five of the most widely used existing methods.

The remainder of this paper is organized as follows: Section 2 introduces the data processing algorithm. Section 3 introduces the experimental design. Section 4 compares and analyzes the proposed and existing methods through experiments. Section 5 is the conclusion.

2. Data Processing Algorithm

2.1. Algorithm Principle

Lithium-ion batteries are often assigned to work within a certain range due to safety and economic considerations [21], and this range is hereinafter referred to as the working range. This study sets the working range as

$$\mathrm{SOC} \in [\mathrm{SOC_L}, \mathrm{SOC_H}], I \in [I_\mathrm{L}, I_\mathrm{H}], T_{bat} \in [T_{batL}, T_{batH}], \tag{3}$$

where the subscripts L and H represent the low and high boundaries of the variables, respectively.

In order to estimate OCV in the whole working range, large-current CCTs under several T_{amb} must be conducted to obtain the necessary data. This study assumes that n CCTs are conducted under each of the m T_{amb}. Thus, a total of $m \times n$ CCTs are performed, and the specific values are expressed as

$$\{I_1, I_2, \ldots, I_n\} \in [I_\mathrm{L}, I_\mathrm{H}], \{T_1, T_2, \ldots, T_m\} \in [T_{batL}, T_{batH}]. \tag{4}$$

With the above data, the main principle of the proposed algorithm is elucidated as follows. For a particular $T_{amb} = T_j \in \{T_1, T_2, \ldots, T_m\}$, the U– and OCV–SOC curves are shown in Figure 3 (assuming $0 < I_1 < I_2 < \ldots < I_n$). It can be seen that as the test currents of the n CCTs decrease, U approaches OCV due to decreasing ΔU. Further, electrochemical theory shows that for CCTs of different I, U is continuous and monotonous with respect to I under a particular {SOC,T_{bat}} [1], so there exists a U–I function. Therefore, this study first estimates the U–I function and then estimates OCV by setting $I = 0$ in the U–I function (referred to as $U(I = 0)$ hereinafter).

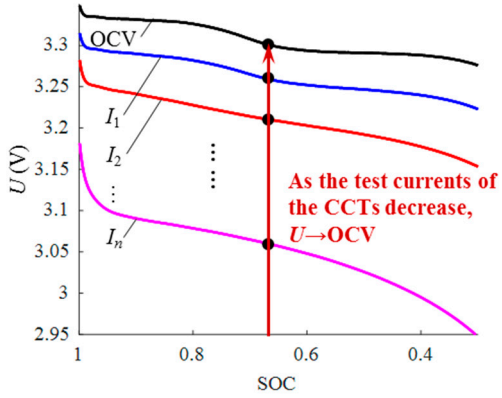

Figure 3. U approaches open circuit voltage (OCV) under the same T_{amb}, as test currents of the constant current tests (CCTs) decrease.

Although the main principle of the algorithm is quite simple, two problems must be solved before implementation.

First, estimating the *U*–*I* function requires *U* data of different *I* under the same {SOC,T_{bat}}. However, due to the T_{bat} changing with *I* problem and different heat generation rates of different *I*, discharging/charging the battery with different *I* to the same SOC results in different T_{bat}, even under the same T_{amb}, as shown in Figure 4. This means the required *U* data for the *U*–*I* function estimation is unavailable from experiments.

Second, an existing study [1] showed that the Δ*U*–*I* relation is complex and nonlinear, and thus directly estimating the *U*–*I* function with large-current data results in a certain error at $I = 0$, which is illustrated in Figure 5. Therefore, accurate estimation of the *U*–*I* function and $U(I = 0)$ requires *U* data from multiple CCTs and especially small-current CCTs. However, small-current CCTs require high-precision equipment and are very time consuming, and moreover, they cannot expose some key characteristics, since the battery mostly works under large-current conditions. This study conducted large-current CCTs and compensated for the error with a data processing algorithm, as shown in Section 2.2.

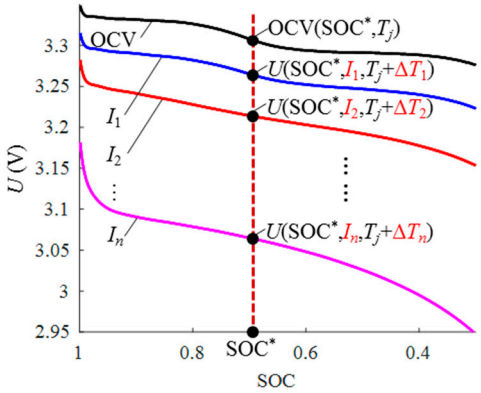

Figure 4. Test *U* data under the same state of charge (SOC) = SOC*, $T_{amb} = T_j$, but different *I* will result in different T_{bat} (Δ*T* stands for T_{bat} changes during operation).

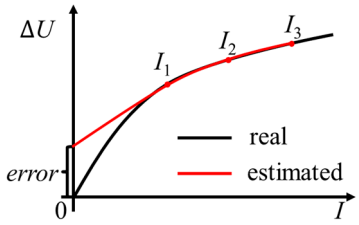

Figure 5. Error at $I = 0$ when estimating the Δ*U*–*I* function with large-current data, due to the nonlinear Δ*U*–*I* relationship.

2.2. Algorithm Procedures

The proposed algorithm was designed with the following steps to solve the above two problems and estimate OCV. The main procedures are shown in Figure 6, and will be introduced in detail as follows.

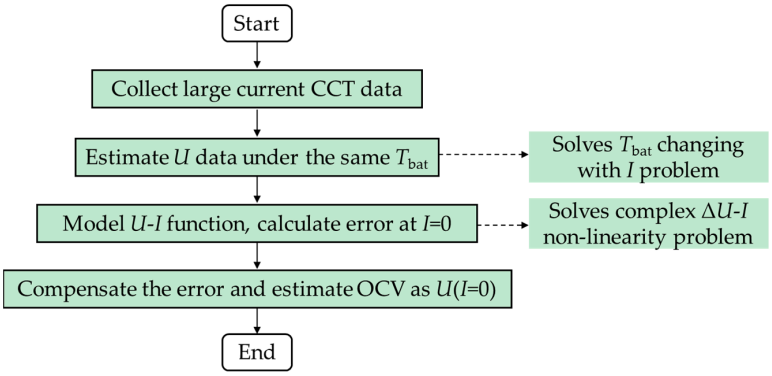

Figure 6. Schematic flow chart of the proposed method.

- Step 1: Collect large-current CCT data.

For ∀SOC ∈ [SOC_L,SOC_H], $m \times n$ U data can be obtained from experiments:

$$\left\{U(\mathrm{SOC}, I_i, T_{ij})\right\}(i = 1,2,3,\ldots,n; j = 1,2,3,\ldots,m), \tag{5}$$

where T_{ij} is the battery temperature when discharging/charging the battery to SOC with $I = I_i$ under $T_{amb} = T_j$.

- Step 2: Estimate U data under the same T_{bat}.

This study proves that U is continuous and monotonous with respect to T_{bat} under a particular {SOC,I}, and details are shown in the Appendix A. So for ∀I_i ∈ [I_1,I_2, … ,I_n], there exists a U–T_{bat} function, and this function is defined as $U = g(T_{bat})|_{SOC,Ii}$. Equation (5) shows that at {SOC,I_i}, there are m U data of different T_{bat}: U(SOC,I_i,T_{ij})(j = 1,2, … ,m). Thus, $g(T_{bat})|_{SOC,Ii}$ can be fit with such data:

$$U(\mathrm{SOC}, I_i, T_{bat}) \approx \hat{U}(\mathrm{SOC}, I_i, T_{bat}) = \hat{g}(T_{bat})\big|_{SOC,I_i}, \tag{6}$$

where the superscript ˆ represents the estimation values after fitting. Then, for ∀T_j ∈ [T_1,T_2, … ,T_m], U(SOC,I_i,T_j) can be estimated as

$$U(\mathrm{SOC}, I_i, T_j) \approx \hat{U}(\mathrm{SOC}, I_i, T_j) = \hat{g}(T_j)\big|_{SOC,I_i}. \tag{7}$$

Therefore, U data of different I under the same {SOC,T_j} can be estimated. At this time, the T_{bat} changing with I problem is solved.

- Step 3: Model U–I function and calculate the error at I = 0.

As mentioned above, there exists a U–I function at {SOC,T_j}, and this function is defined as $U = f(I)|_{SOC,Tj}$. $f(I)|_{SOC,Tj}$ can be estimated through curve fitting with n data from Step 2, $\hat{U}$(SOC,I_i,T_j) (I = 1,2, … ,n). This estimated function is defined as $\hat{f}_{largeI}(I)|_{SOC,Tj}$, where the subscript largeI represents the function fit with large-current CCT data. Then OCV at {SOC,T_j} can be estimated by setting I = 0 in $\hat{f}_{largeI}(I)|_{SOC,Tj}$. However, the Tafel equation [1] shows that estimating OCV with U data from large-current CCTs will result in an error:

$$\mathrm{OCV}(\mathrm{SOC}, T_j) = \hat{f}_{largeI}(I)\big|_{SOC,T_j,I=0} + a(\mathrm{SOC}, T_j), \tag{8}$$

where a is the error, which is a function of SOC and T_{bat}. This study finds that a is not sensitive to SOC, which will be verified in Section 3.2.1. Therefore, a can be considered to be independent of SOC from an engineering point of view. Therefore,

$$\mathrm{OCV}(\mathrm{SOC}, T_j) \approx \hat{\mathrm{OCV}}(\mathrm{SOC}, T_j) = \hat{f}_{largeI}(I)\big|_{SOC,T_j,I=0} + a(T_j), \tag{9}$$

where $\hat{OCV}(SOC, T_j)$ is the estimation result of OCV(SOC,T_j).

Since a is independent of SOC from an engineering point of view, this study can calculate a through measuring the true OCV at only one SOC point (define as SOC_{ref}) under the same T_j and then calculate the error of $\hat{f}_{largeI}(0)|_{SOC,Tj}$. After the true OCV at SOC_{ref} is measured, $a(T_j)$ can be calculated as

$$a(T_j) = OCV(SOC_{ref}, T_j) - \hat{f}_{largeI}(0)\big|_{SOC_{ref},T_j}. \quad (10)$$

- Step 4: Compensate for the error and estimate OCV as $U(I = 0)$.

The error can be compensated for and OCV can be estimated as

$$\hat{OCV}(SOC, T_j) = \hat{f}_{largeI}(0)\big|_{SOC,T_j} + OCV(SOC_{ref}, T_j) - \hat{f}_{largeI}(0)\big|_{SOC_{ref},T_j}. \quad (11)$$

At this point, the U–I function is modeled and the modeling error at $I = 0$ caused by ΔU–I nonlinearity is compensated for. Therefore, OCV can be estimated through large-current CCTs and very few OCV measurement experiments, with a shortened experimental time and adequate accuracy.

3. Experimental Design

This section introduces the experimental design of the proposed method. It is worth noting that the experiments here contained a large amount of redundancy. The purpose of such redundancy was to provide experimental parameter design suggestions for the proposed method that suit other lithium-ion batteries of similar characteristics as well. The required experiments in actual applications were much less, as can be found at the end of Section 4.1.

3.1. Example of Experimental Procedures

The proposed method mainly conducted large-current CCTs. A few OCV true value measurement tests were also conducted to compensate for the U–I modeling error, as mentioned in Section 2.2. The procedures of these tests are illustrated through examples in Section 3.1.1. and Section 3.1.2., respectively.

This study used a battery test system (type: BTS-4) from Neware Company to charge and discharge the battery, and used a thermal chamber to control T_{amb}. This study used a BAK Company 3-A·h lithium iron phosphate battery, whose parameters are shown in Table 1.

The working range of batteries should be determined according to application requirements. For a simplification of the description, this study set the working range as an example:

$$SOC \in [0.3, 1], I \in [0, 2.5], T_{bat} \in [0, 60]^{\circ}C. \quad (12)$$

Table 1. Battery parameters.

Parameters	Value
Type	26650MP2-Fe
Electrode material	LiFePO4/Graphite
Nominal capacity/Ah	3
Maximum constant charging current/C [1]	2
Maximum constant discharging current/C	3

[1] C means C rate, where 1 C = 3 A.

3.1.1. Constant Current Test Procedures

CCTs were conducted with multiple I and T_{amb} in this example. The specific values are listed in Table 2, that is, a total of 36 CCTs. The charging of all CCTs was conducted at T_{amb} = 25 °C (the

standard temperature specified by the battery manufacturer) to ensure SOC = 1 at the beginning of discharge. Specifically, each CCT consisted of the following steps:

(1) Charge the battery using the standard procedures from the battery manufacturer. That is, charge the battery with $I = -0.5$ C, then start constant voltage charging when $U = 3.6$ V. Charging is completed when $I = -0.02$ C;
(2) Immediately after charging is completed, change T_{amb} from 25 °C to T_j ($T_j \in \{5,15,25,35,45,55\}$ °C and rest the battery for 2.5 h to make $T_{bat} = T_j$ and the battery's internal processes steady;
(3) Discharge the battery with I_i ($I_i \in \{0.2,0.6,1.0,1.4,1.8,2.2\}$ C). Discharging is completed when $U = 2.5$ V;
(4) Immediately after discharge is completed, adjust T_{amb} to 25 °C and rest the battery for 0.5 h to let the internal processes approach steady. Then start the next CCT.

Table 2. Specific value of experiment I and T_{amb}.

I/C [1]	T_{amb}/°C
0.2/0.6/1.0/1.4/1.8/2.2	5/15/25/35/45/55

[1] C means C rate, where 1 C = 3 A.

Notably, rest time needs to be determined according to the volume and shape of the battery. The larger the volume is, the more inconvenient the shape is for heating diffusion, so the more rest time there should be. This study verified that the above rest time was sufficient for the battery used here.

3.1.2. OCV True Value Measurement Test Procedures

This study measured the OCV true value corresponding to SOC_{ref} under the above T_j due to the need for U–I modeling error compensation. Specifically, the fully charged battery was discharged to $SOC_{ref} = 0.9$ and was then rested for 1 h at each T_j. The U at the end of the rest was taken as the OCV true value.

3.2. Experimental Parameter Design

As mentioned above, this study conducted n CCTs under m T_{amb} and measured the OCV true value corresponding to SOC_{ref} under each T_{amb}. That is, a total of three sets of parameters needed to be designed: (1) the specific value of SOC_{ref}; (2) the specific value of $\{I_1,I_2,\ldots,I_n\}$ and number n; and (3) the specific value of $\{T_1,T_2,\ldots,T_m\}$ and number m.

So far, the experimental parameter designs of the existing methods have been mostly empirical or have been designed in combination with the actual working conditions of the battery [13–20]. This is because a battery's characteristics and applications are so different that it is very hard to provide "optimal" experimental parameters that fit all batteries and applications. However, experimental parameters do have an important impact on estimation accuracy and experimental time. This section combines the battery mechanism and actual experimental data to analyze the experimental parameters' influence on estimation accuracy and experimental time, and then proposes experimental parameter design suggestions.

The true value of the OCV is needed to analyze estimation accuracy. This section took the HPPC results as the OCV true value, since the HPPC method is adequately accurate [14]. The specific analyses were as follows.

3.2.1. SOC_{ref} Design

SOC_{ref} Influence on Estimation Accuracy

In order to study the influence on estimation accuracy, eight SOC_{ref} were uniformly selected in the working range (i.e., SOC_{ref} = 1.0, 0.9,..., 0.3) and other experimental parameters were set to fixed

values (as an example, T_{amb} = 5, 15, 25, 35, 45, 55 °C, I = 0.2, 0.6 C). The maximum and the average estimation error corresponding to the above SOC_{ref} are shown in Figure 7.

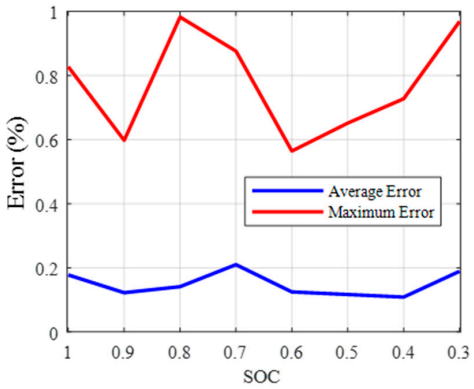

Figure 7. Average and maximum estimation error of different SOC_{ref}.

Two conclusions could be drawn from Figure 7: (1) the estimation accuracy of all of the above SOC_{ref} was high from an engineering point of view, where the maximum error was less than 0.98% and the average error was less than 0.21%; and (2) the error was relatively small when SOC_{ref} was near 0.9 and 0.4–0.6.

Conclusion 1 verified the conclusion that the modeling error a could be treated independently of SOC from an engineering point of view, as mentioned in Step 3, Section 2.2. Although this study could not prove its rationality in a mechanistic way, the study did use a variety of batteries of different materials, capacities, and aging statuses to conduct the experiments, and the actual experimental data showed this compensation was very accurate in an engineering sense.

Conclusion 2 showed that setting SOC_{ref} reasonably could further improve estimation accuracy. As mentioned earlier, estimation accuracy was higher when SOC_{ref} was around 0.9 and 0.4–0.6, where it exactly corresponded to the voltage platform of the constant current discharge U–SOC curve. In the voltage platform, the internal reaction of the battery was relatively stable, which was probably the reason the compensation accuracy was higher. The reasons for the lower estimation accuracy of other SOC_{ref} were (1) when SOC_{ref} = 1, the current excitation had just been applied and the dynamics of Z were still unstable, which made the derivations in Section 2 invalid; (2) SOC_{ref} = 0.7–0.8 was the phase transition region of the lithium iron phosphate battery [16], and phase transition information is often not very obvious in U data in large-current CCTs; and (3) there was also a phase transition region near SOC_{ref} = 0.3 [16].

This study used a variety of LPF/C (LiFePO4/Graphite) lithium-ion batteries for experiments and found that SOC = 0.9 or 0.4–0.6 was a common area where the voltage platform occurred. For another commonly used NCM/C (Nickel-Cobalt-Manganese/Graphite) lithium-ion battery, the voltage platform's position varied with different material ratios and battery aging states, but near SOC = 0.9, the voltage platform was often obvious for different material ratios throughout the whole lifespan. Therefore, setting SOC_{ref} = 0.9 could improve estimation accuracy.

SOCref Influence on Experimental Time

SOC_{ref}'s influence on the experimental time was reflected in the time used to discharge the battery from SOC = 1 to SOC_{ref}, as shown in Section 3.1.2. Obviously, the closer SOC_{ref} was to 1, the shorter the experimental time was. For example, an I = 0.5 C discharge to SOC_{ref} = 0.9 took about 12 min, while SOC_{ref} = 0.5 took about 1 h.

Considering SOC_{ref}'s influence on estimation accuracy and experimental time, setting SOC_{ref} = 0.9 could improve estimation accuracy and shorten the experimental time at the same time for LPF/C and NCM/C lithium-ion batteries, so this study suggests SOC_{ref} be set to 0.9, approximately.

3.2.2. Design of Specific Value of $\{I_1,I_2,\ldots,I_n\}$ and Number n

Design of Number n

The larger n is, the longer the experimental time is. Therefore, n should be set as small as possible as long as estimation accuracy is ensured. The n minimum takes 2 to linearly model the nonlinear U–I relation, so this study first compared the estimation accuracy of n = 2 and 3. It could be assumed that $|I_1|<|I_2|<|I_3|$ for any $\{I_1,I_2,I_3\}$. Only $\{I_1,I_2\}$ and $\{I_1,I_2,I_3\}$ needed to be compared, since other cases should be analyzed as the influence of current specific values. This section takes an example for convenience of description. The conclusions derived from this example were representative, as verified by this study. $\{I_1,I_2,I_3\}$ were set as {0.2,0.6,1.0}, and other parameters were set as SOC_{ref} = 0.9, T_{amb} = 5, 15, 25, 35, 45, 55 °C in the example. A comparison of the estimation results is shown in Figure 8.

It can be seen from Figure 8 that the estimation accuracy with n = 3 was almost the same as with n = 2. Specifically, the average estimation errors of n = 2 and 3 were 0.12% and 0.14%, respectively, and the maximum estimation errors were 0.60% and 0.90%, respectively. From a mechanism point of view, increasing n should increase estimation accuracy as long as no overfitting occurs, since the U–I relationship is nonlinear and complex. However, n = 2 could already achieve adequate accuracy, since this study designed an algorithm to compensate for the modeling error caused by U–I nonlinearity. On the other side, increasing n significantly increased experimental time. In this example, the experimental time of n = 2 and 3 was 18 h and 24 h, respectively, which was a 33.3% difference. To sum up, this study suggests setting n = 2, in consideration of both estimation accuracy and experimental time.

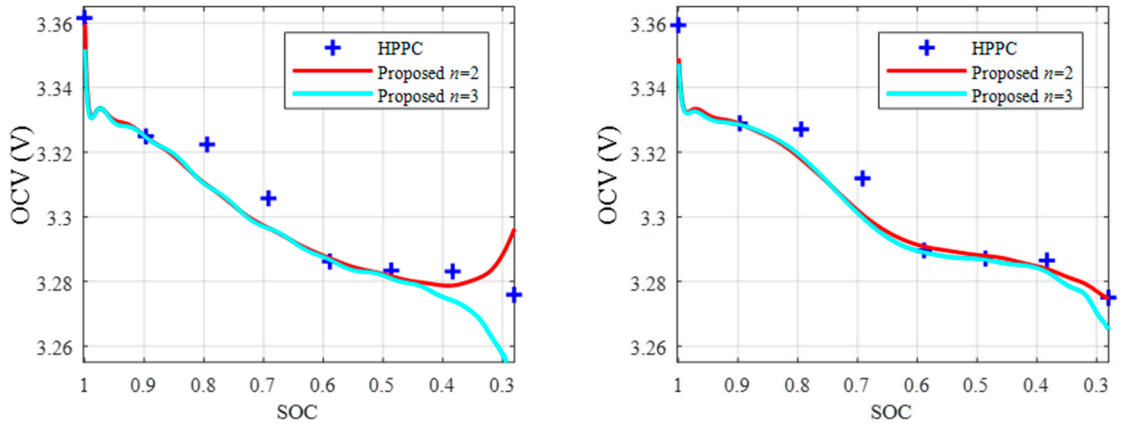

(**a**) T_{bat} = 5 °C (**b**) T_{bat} = 15 °C

(**c**) T_{bat} = 25 °C (**d**) T_{bat} = 35 °C

Figure 8. *Cont.*

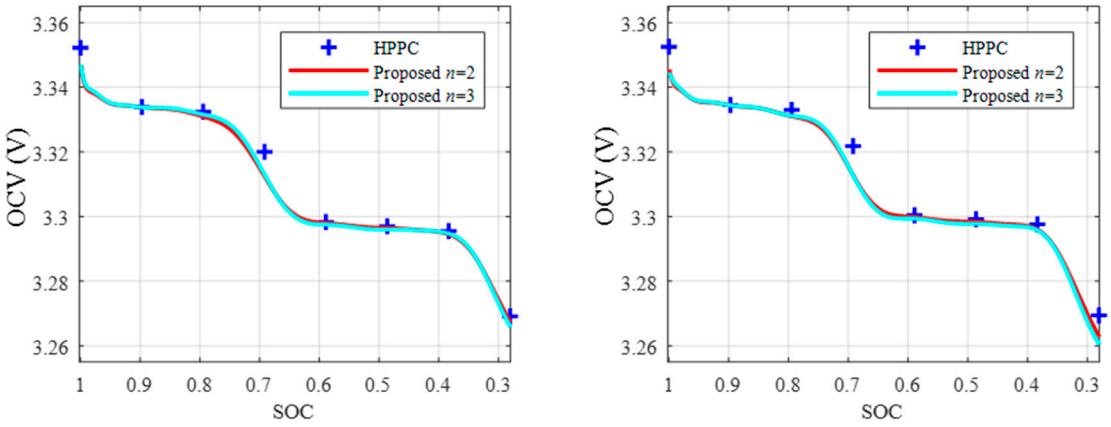

(**e**) T_{bat} = 45 °C (**f**) T_{bat} = 55 °C

Figure 8. Estimation results of the hybrid pulse power characterization (HPPC) method and the proposed method, with n = 2 and 3, respectively. (**a**) T_{bat} = 5 °C; (**b**) T_{bat} = 15 °C; (**c**) T_{bat} = 25 °C; (**d**) T_{bat} = 35 °C; (**e**) T_{bat} = 45 °C; (**f**) T_{bat} = 55 °C.

Design of Specific Value of $\{I_1, I_2, \ldots, I_n\}$

While designing the current specific values, other parameters were set as SOC_{ref} = 0.9, n = 2, and T_{amb} = 5, 15, 25, 35, 45, 55 °C, based on the previous conclusions. There were C_6^2= 15 cases of $\{I_1, I_2\}$, since $\{I_1, I_2\} \subset \{0.2, 0.6, 1.0, 1.4, 1.6, 2.2\}$. This study studied all of the cases, but only shows the necessary results due to space limitations. Figure 9 shows the estimation results when I_1 = 0.2 C and I_2 is another current. It can be seen that I_2 had little impact on estimation accuracy in the high-T_{bat} and high-SOC region. However, estimation accuracy decreased with increasing I_2 in the low-T_{bat} and low-SOC region. Similarly, this study studied the influence of I_1 on estimation accuracy and concluded that I_1 had little influence on estimation accuracy in the high-T_{bat} and high-SOC region, but estimation accuracy decreased with increasing I_1 in the low-T_{bat}, low-SOC region.

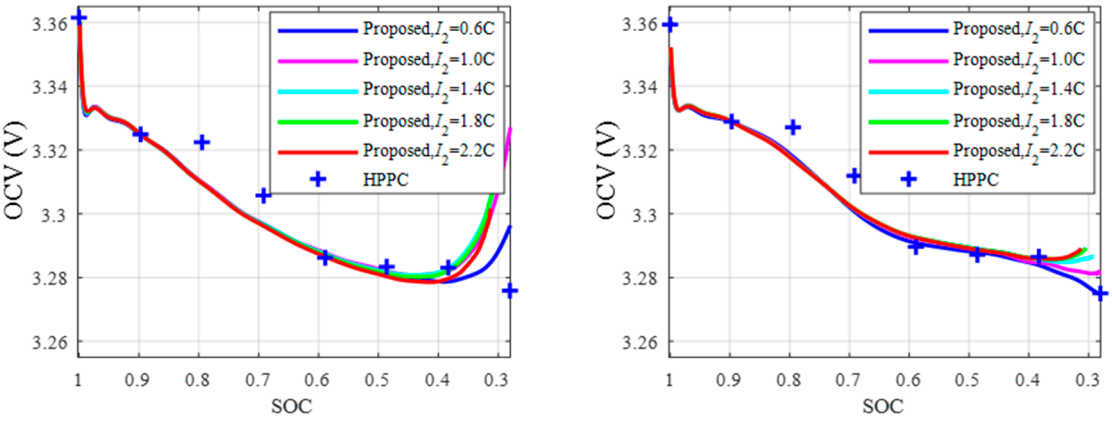

(**a**) T_{bat} = 5 °C (**b**) T_{bat} = 15 °C

Figure 9. *Cont.*

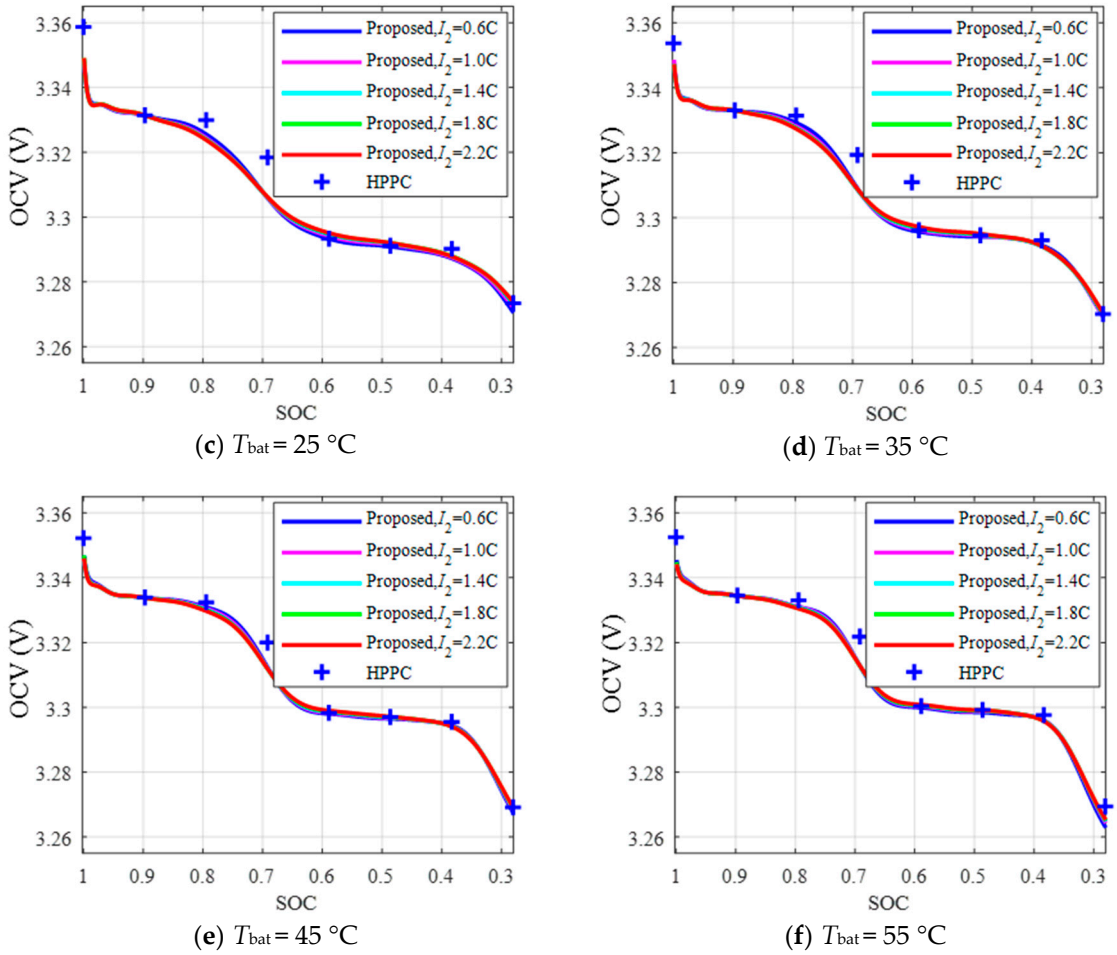

Figure 9. Estimation results of the HPPC method and the proposed method of different I_2 (I_1 = 0.2 C, where C means the C rate). (**a**) T_{bat} = 5 °C; (**b**) T_{bat} = 15 °C; (**c**) T_{bat} = 25 °C; (**d**) T_{bat} = 35 °C; (**e**) T_{bat} = 45 °C; (**f**) T_{bat} = 55 °C.

This study attempted to estimate $U(I = 0)$ as the OCV. Therefore, the smaller I was, the higher the estimation accuracy should have been, but the longer the experimental time was. Therefore, there was a trade-off between estimation accuracy and experimental time. For example, the maximum estimation errors of $\{I_1,I_2\}$ = {0.2,0.6}, {0.2,1.0}, {0.6,1.0} were 0.6%, 1.5%, 6.3%, and the experimental time under each T_{amb} was 18 h, 17.5 h, 14 h. Therefore, this study could not quantitatively determine the optimal values of I, since different applications have different requirements for estimation accuracy and experimental time. However, this study could provide some design suggestions qualitatively:

(1) I should not be too large or too small, due to the trade-off between estimation accuracy and experimental time;

(2) If the working temperature is low, I should be set to be smaller to guarantee estimation accuracy. As shown in Figure 9, estimation accuracy was lower at low temperatures. This was mainly due to an increase in a battery's concentration polarization at low temperatures, which led to an increase of ΔU in the CCTs, so it was more difficult to model the U–I function accurately;

(3) If the working range contains a low-SOC region, I should be set to be smaller. The reason is similar to item (2), that is, a battery's ΔU is larger at low SOCs;

(4) If the battery ages seriously, I should be set to be smaller. The reason is similar to item (2), that is, an aged battery's ΔU is larger.

This study used a variety of batteries of different materials and aging statuses to conduct the experiments. The experimental results indicated that for most engineering applications, I_1 should be

<0.5 C, and I_2 should be larger than I_1 but no larger than 1 C. Specific values should be determined according to a battery' characteristics and application needs.

3.2.3. Design of the Specific Value of $\{T_1, T_2, \ldots, T_m\}$ and Number m

Experiments under a few T_{amb} were conducted to estimate OCV(SOC,T_{bat}) in the working range, as mentioned above. This study could not quantitatively provide the T_{amb} setting principle that is applicable to all conditions, since the requirements and working range of different applications are different. However, this section provides some qualitative design tips based on a battery's actual characteristics and electrochemical mechanism.

Other experimental parameters were set as SOC_{ref} = 0.9, $\{I_1,I_2\}$ = {0.2,0.6}, as discussed above. An estimation result at SOC = 0.9 is provided as an example here for convenience of description. Specifically, the OCV–T_{bat} relation at SOC = 0.9 is shown in Figure 10.

It can be seen that OCV increased monotonously with an increase in T_{bat}, but the increasing rate gradually decreased. Therefore, the specific value of T_{amb} should cover the entire working range, but more experiments should be conducted at low temperatures since OCV is more sensitive to T_{bat} there.

The number m must be determined according to application requirements. The larger m is, the higher the estimation accuracy is, since the OCV–T_{bat} relation is calculated through curve fitting or interpolation. However, experimental time is approximately proportional to m, since the experiments conducted under different T_{amb} were almost the same. That is, the setting of m is a trade-off between estimation accuracy and experimental time. Thus, m should be set according to actual application requirements. According to the authors' experience, m should be set to at least 3~4 if the working temperature range is as wide as this example.

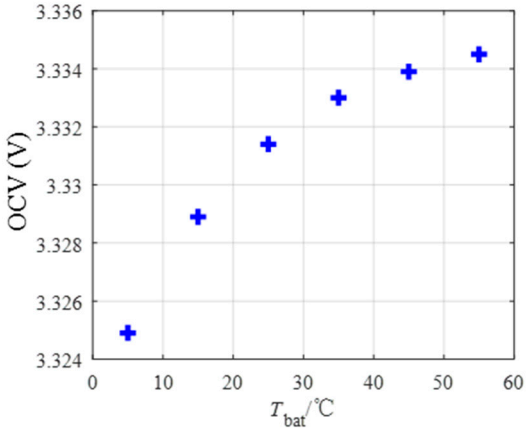

Figure 10. OCV–T_{bat} relation at SOC = 0.9.

4. Comparison between Different Methods

This section compares the proposed method with the five most widely used existing OCV estimation methods: the long time rest (LTR) method [13], HPPC method [14], terminal voltage prediction (TVP) method [17], small-current approximation (SCA) method [20], and terminal voltage average (TVA) method [19]. The first three methods are VR methods, and the latter two and the proposed method are CC methods. Three important performance indicators of concern in applications were chosen as evaluation criteria: estimation accuracy, experimental time, and also other battery information obtained, since real applications usually require various types of battery information at the same time.

A summary sheet is shown in Table 3. In Table 3, the experimental procedures and parameters of the proposed method are those from Sections 3.1 and 4.1, respectively, and the algorithm of the proposed method is from Section 2.2. The other methods' experiments and algorithm can be found

in Section 3.2, References [13–17] and [18–20]. Further details from Table 3 will be explained in the remainder of this section.

Table 3. Comparisons between different methods.

Methods	Error Max	Error Mean	Experimental Time [1]/hour Estimation Results at 10/20/1000 SOC Points			Other Information
LTR	taken as true value		208	408	20008	Impedance
HPPC	0.45%	0.19%	19	29	1009	Impedance
TVP	0.40%	0.22%	11.7	15	341.7	Impedance
SCA	1.08%	0.52%	30	30	30	capacity with small-current conditions, ICA information
TVA	3.60%	0.92%	55	55	55	capacity/resistance with small-current conditions, ICA information
Proposed	0.45%	0.20%	18	18	18	capacity/resistance with normal-current condition, thermal characteristics, ICA information

[1] This study compared each method's experimental time when estimating OCV at 10/20/1000 SOC points, since different applications require different amounts of OCV estimation results under each T_{bat}. LTR: long time rest; TVP: terminal voltage prediction; SCA: small-current approximation; TVA: terminal voltage average; ICA: incremental capacity analysis.

4.1. Experiments for Method Comparison

This section conducts multiple experiments with the above six methods. The battery working range was as shown in Equation (12). The specific experiments were as follows.

The LTR method [13] rests the battery for 20 h at a particular {SOC,T_{bat}} and takes the U at the end of the rest as the OCV. Limited by experimental time, this study only conducts the 20-h rest for a small portion of SOC points. Specifically, rest experiments were conducted at SOC = 0.9, 0.65, T_{amb} = 5, 15, 25, 40 °C.

The HPPC method [14] rests the battery for 1 h at a particular {SOC,T_{bat}} and takes the U at the end of the rest as the OCV. Specifically, rest experiments were conducted at SOC = 1.0, 0.9, . . . , 0.3, T_{amb} = 5, 15, 25, 40 °C.

The TVP method [17] rests the battery for 20 min at a particular {SOC,T_{bat}} and models the U–t function during rest. The TVP method predicts the U after 20 h of rest and takes it as the OCV. The specific experiment was very similar to HPPC. The only difference was that the rest time was changed from 1 h to 20 min.

The SCA method [20] takes the U of the small-current CCT as the OCV. Therefore, a I = 1/25 C CCT was conducted at T_{amb} = 5, 15, 25, 40 °C. For specific experimental procedures, refer to Section 3.1.1.

The TVA method [19] takes the average U of two small-current CCTs as the OCV. The currents of the two CCTs are of the same amplitude but in opposite directions. In this study, I = ±1/25 C CCTs were conducted at T_{amb} = 5, 15, 25, 40 °C. For specific experimental procedures, refer to Section 3.1.1.

The proposed method's experimental procedures were introduced in Section 3.1. The specific experimental parameters were set as SOC_{ref} = 0.9, I = 0.2, 1/3 C, and T_{amb} = 5, 15, 25, 40 °C, according to the conclusions of Section 3.2.

4.2. Comparision and Analysis

This section compares three performance indicators of the above methods: estimation accuracy, experimental time, and other battery information obtained. The details are as follows.

4.2.1. Estimation Accuracy

Estimation results of the above methods are shown in Figure 11. A quantitative comparison of estimation accuracy requires a true value. U, after a battery rests for a long time, can be taken as the

OCV from an engineering point of view [13], which is the case with the LTR method. The estimation error of each method is shown in Figure 12.

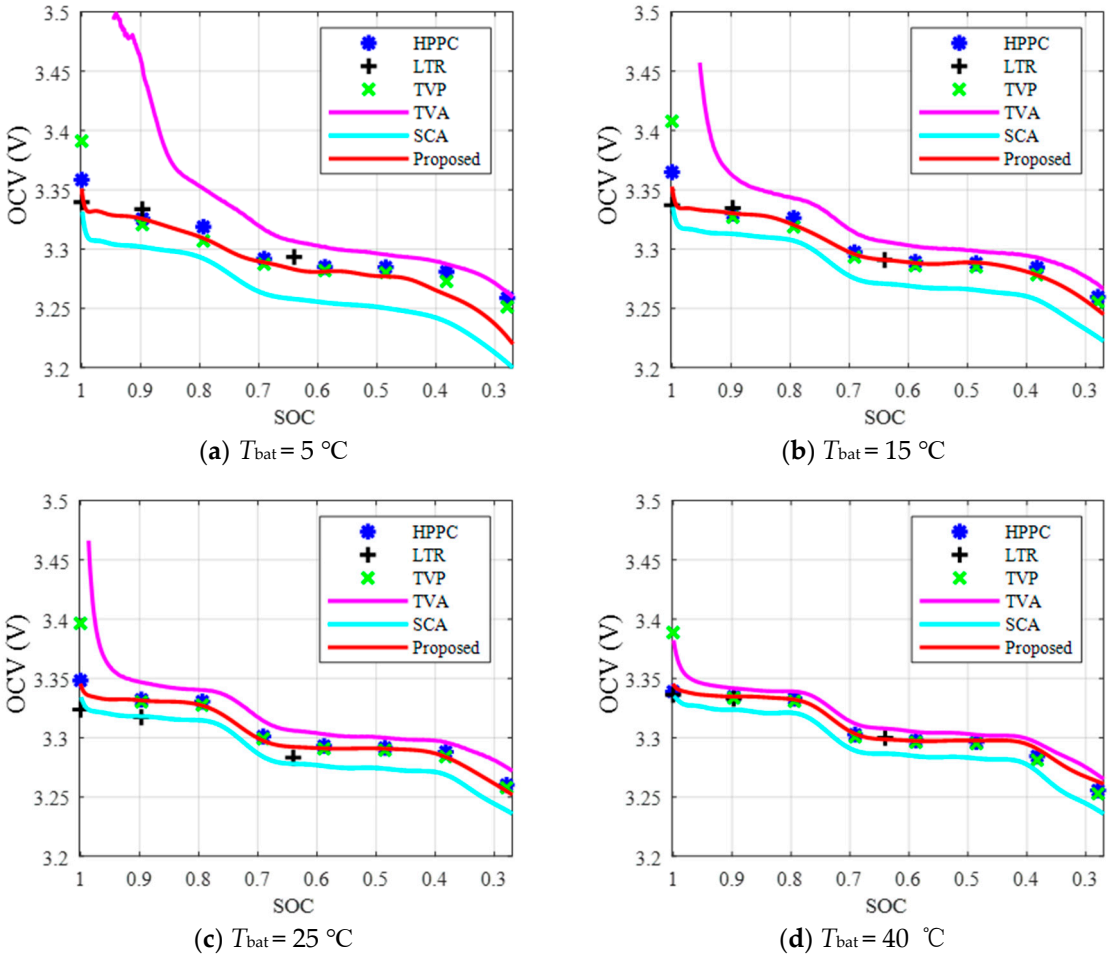

Figure 11. Estimation results of different methods. (**a**) T_{bat} = 5 °C; (**b**) T_{bat} = 15 °C; (**c**) T_{bat} = 25 °C; (**d**) T_{bat} = 35 °C.

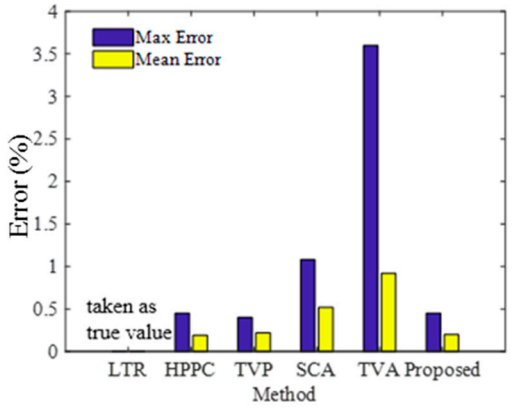

Figure 12. Estimation errors of different methods.

It can be seen that the overall estimation accuracy of the proposed method was high, and the error was only slightly higher in the low-T_{bat} and low-SOC region. The HPPC method had high estimation accuracy in the whole working range. The TVP method's estimation accuracy was slightly lower than the HPPC method, but was still high. The estimation result of the SCA method was relatively low in

the whole working range. The estimation result of the TVA method was relatively high, especially in the low-T_{bat} and high-SOC region.

To sum up, the estimation accuracies of the proposed, HPPC, and TVP methods were high, but the estimation accuracies of the SCA and TVA methods were relatively low. Due to space limitations, this study will not analyze the source of error of each method and the cause of the above results.

4.2.2. Experimental Time

The experimental time required to estimate the OCV–SOC curve at one T_{bat} is compared here, for convenience of description. Different applications require different amounts of estimation results at each T_{bat}: For instance, SOC estimation [4] requires OCV estimation results at 10–20 SOC points, but the ICA [19] requires OCV estimation results at a minimum of 1000 SOC points. Therefore, the experimental time required to estimate OCV at 10, 20, and 1000 SOC points through each method were compared. The details are shown in Figure 13 (part of the experimental time was reasonably inferred from actual experimental data).

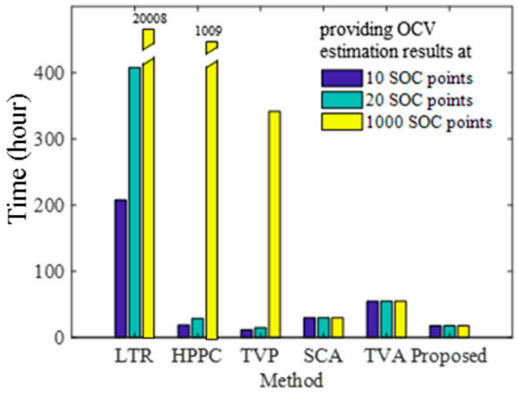

Figure 13. Experimental times of different methods.

It can be seen that the experimental times of the LTR, HPPC, and TVP methods increased linearly with the number of estimation results, because all three VR methods require a rest experiment at each SOC. The experimental times of the SCA, TVA, and proposed methods were independent of the number of estimation results. This was because these three CC methods conduct CCTs that can collect large amounts of test data at different SOC points, due to the high sampling frequency of test equipment. For example, an I = 1/3 C CCT takes about 3 h. If the sampling frequency is 1 Hz, the CCT can collect experimental data of about 10,800 SOC points.

Therefore, a quantitative comparison of these methods relates to application needs. Nowadays, SOC estimation application requires an accuracy of about 2%~5% [22], and therefore OCV estimation results of at least 20 SOC points usually need be provided. At this point, the TVP and proposed method consumed significantly less experimental time than the other methods did. It can be seen from Figure 13 that the proposed method only consumed 16.7% more experimental time than the quickest existing method (TVP) did, which means the proposed method's experimental time suited SOC estimation application quite well. For another application, ICA, OCV estimation results of at least 1000 SOC points are needed. At this point, the proposed, SCA, and TVA methods consumed significantly less experimental time than the other methods did. Among these three methods, the proposed method was the quickest and only consumed 60.0% and 32.7% of the experimental time of the SCA and TVA methods, respectively.

To sum up, the TVP and proposed methods consumed the least experimental time in applications that required very few OCV estimation results under each T_{bat}, such as SOC estimation applications. The proposed method consumed the least experimental time in applications that required a detailed OCV–SOC curve, such as ICA in SOH (state of health) estimation applications. This means the

proposed method's experimental time suits both applications quite well. It is also necessary to note the above analyses were based on the premise that all data of the proposed method must be collected from experiments. The proposed method will have more of an advantage in experimental time when other large-current CCT data is available, such as online constant-current charging data.

4.2.3. Other Battery Information

The information obtained for each method was mainly determined by the battery characteristics excited by its experiment. The details are as follows.

The proposed method conducts CCTs with different I and could obtain the available capacity/energy at different I. In addition, due to the large current used in the experiment, internal resistance at the large-current working point could be obtained (see Reference [23] for details), and thermal characteristics and thermal model parameters of the battery could be further obtained. The above information is very important for understanding the actual working characteristics of the battery, since the current amplitude of this method is close to a battery's actual working current. Moreover, the ICA could be further conducted to analyze the internal changes of the battery during aging, since the method could provide detailed OCV–SOC estimation results. However, as CCTs contain little dynamic excitations, the proposed method could not provide impedance information, except at SOC = 1, when the experimental current was just applied to the battery.

The TVA method and SCA method also conducted CCTs, but the current amplitude was very small. These two methods could obtain battery available capacity/energy and internal resistance information in small-current conditions. This information is more suitable for theoretical analysis, since the current amplitude of these methods was much smaller than the actual working current. These methods could not be used to analyze the thermal characteristics of the battery, since heat generation in the small-current experiment was not obvious. As mentioned earlier, these two methods could be used for ICA but could not provide impedance information.

The LTR, HPPC, and TVP methods used step signal excitation multiple times in the experiment. These methods could obtain the impedance of the battery, since step excitation contains more dynamic signals. However, the excitation duration was too short to excite the battery thermal characteristics significantly, although large-current excitation was used in the experiment. At the same time, these methods did not apply to the ICA due to great experimental time consumption.

It can be seen that the information obtained by the proposed method was almost the total of the other five methods, except for impedance. Moreover, the proposed method could also provide thermal parameters, which the other five methods could not.

5. Conclusions

This paper proposes a time-efficient and adequately accurate OCV(SOC,T_{bat}) estimation method for engineering applications of lithium-ion batteries. Large-current CCTs were conducted to collect enough data in a time-efficient way. A set of algorithms based on battery electrochemical mechanisms was designed to solve T_{bat} changing with I and complex ΔU–I nonlinearity problems and therefore estimate the OCV(SOC,T_{bat}) with enough accuracy. Moreover, the experimental design principles were provided in this paper for researchers to design experiments specifically according to application requirements. The experimental results are summarized in Table 3, which shows the proposed method had a great advantage considering comprehensive factors such as experimental time, estimation accuracy, and other battery information obtained:

(1) For applications that require detailed OCV–SOC curves, the proposed method only consumes 5.3%/60% of the experimental times of the fastest VR/existing CC methods. For applications that require rough OCV–SOC curves, the proposed method consumes almost the same/60% of the experimental times of the fastest VR/existing CC methods;

(2) The average and maximum estimation errors of the proposed method are 0.20% and 0.45%, respectively. This indicates that the proposed method has accuracy similar to VR methods and has higher accuracy than existing CC methods;

(3) The proposed method provides a lot of other battery information at the same time, such as a battery's capacity, resistance, aging status, and uniquely thermal parameters that existing OCV estimation methods cannot provide. The provided information is almost the total of existing OCV estimation methods, except for impedance.

These characteristics make the proposed method very suitable for engineering applications such as battery aging evaluation, which requires accurate, detailed, and plentiful information in a time-efficient way. Optimization (such as providing impedance information at the same time) of the proposed method will be carried out in future work.

Author Contributions: Y.C. proposed the original idea, conceived the experiments, and analyzed the data. G.Y. helped to develop the original idea and revised the manuscript. X.L. carried out the experiments and revised the manuscript. Z.H. revised the manuscript.

Funding: This research was funded by the National Key R&D Program of China under Grant 2016YFB0900302 and the National Natural Science Foundation of China (NSFC) under Grant U1510208, 61273045.

Conflicts of Interest: The authors declare no conflicts of interest.

Nomenclature

a	OCV estimation error with large-current experimental data
Ah	ampere hour
C	C rate, per unit of experimental current
CC	constant current
CCT	constant current test
C_{nom}	nominal capacity
ECM	equivalent circuit model
$f(I)\vert_{\mathrm{SOC},Tj}$	U–I function at {SOC,T_j}
$\hat{f}_{\mathrm{largeI}}(I)\vert_{\mathrm{SOC},Tj}$	fitted $f(I)$ with large-current experimental data
$g(T_{\mathrm{bat}})\vert_{\mathrm{SOC},Ii}$	U–T_{bat} function at {SOC,I_i}
HPPC	hybrid pulse power characterization
ICA	incremental capacity analysis
I	working current
I_1, I_2, I_3, I_i, I_n	specific experiment current
I_{L}	minimum I in working range
I_{H}	maximum I in working range
LTR	long time rest
LPF/C	LiFePO4/Graphite
m	number of experimental ambient temperatures
n	number of experimental currents
NCM/C	Nickel-Cobalt-Manganese/Graphite
OCV	open circuit voltage
SCA	small-current approximation
SOC	state of charge
$\mathrm{SOC_L}$	minimum SOC in working range
$\mathrm{SOC_H}$	maximum SOC in working range
SOC^*	a specific state of charge
$\mathrm{SOC_{ref}}$	state of charge where OCV is measured
t	operation time
t_0	start time of the operation
T_1, T_2, T_j, T_m	specific temperature
T_{ij}	T_{bat} when discharging/charging the battery to SOC with $I = I_i$ under $T_{\mathrm{amb}} = T_j$.
ΔT	T_{bat} changes during operation
T_{amb}	ambient temperature

T_{bat}	battery temperature
T_{batL}	minimum T_{bat} in working range
T_{batH}	maximum T_{bat} in working range
TVA	terminal voltage average
TVP	terminal voltage prediction
U	terminal voltage
$U(I = 0)$	terminal voltage when $I = 0$ in the CCT
ΔU	terminal voltage drop
VR	voltage relaxation
Z	equivalent impedance
^	estimated value

Appendix A : Proof That the U–T_{bat} Relation Is Continuous and Monotonic

In the CCTs, Z can be simplified as an internal resistance R, which is a time-varying function of SOC, I, and T_{bat}. Therefore, Equation (1) turns into

$$\begin{gathered} \text{For constant current conditions :} \\ U(\text{SOC}, I, T_{bat}) = \text{OCV}(\text{SOC}, T_{bat}) - \Delta U(\text{SOC}, I, T_{bat}) \\ \Delta U(\text{SOC}, I, T_{bat}) = R(\text{SOC}, I, T_{bat}) \times I \end{gathered} . \tag{A1}$$

The Nernst equation shows that the OCV–T_{bat} relationship is continuous and monotonic [1]. The Butler–Volmer equation and other existing electrochemical theory show that the R–T_{bat} relationship is also continuous and monotonic [1]. Moreover, actual characteristics of the battery indicate that R is much more sensitive to T_{bat} than OCV [24,25]:

$$\frac{\partial \text{OCV}(\text{SOC}, T_{bat})}{\partial T_{bat}} > 0, \frac{\partial R(\text{SOC}, I, T_{bat})}{\partial T_{bat}} < 0, \left|\frac{\partial R(\text{SOC}, I, T_{bat})}{\partial T_{bat}}\right| \gg \left|\frac{\partial \text{OCV}(\text{SOC}, T_{bat})}{\partial T_{bat}}\right|. \tag{A2}$$

Therefore, it can be derived from Equation (A1) that the U–T_{bat} relationship is also continuous and monotonic, except for in the case of charging with extremely small currents (which does not happen in this method):

$$\begin{gathered} \frac{\partial U(\text{SOC}, I, T_{bat})}{\partial T_{bat}} = \frac{\partial \text{OCV}(\text{SOC}, T_{bat})}{\partial T_{bat}} - I \times \frac{\partial R(\text{SOC}, I, T_{bat})}{\partial T_{bat}} \\ \text{if } I > 0, \text{ then } \frac{\partial U(\text{SOC}, I, T_{bat})}{\partial T_{bat}} > 0 \\ \text{if } I < 0 \text{ and } I \neq \text{infinitesimal, then } \frac{\partial U(\text{SOC}, I, T_{bat})}{\partial T_{bat}} < 0 \end{gathered} . \tag{A3}$$

References

1. Bard, A.J.; Faulkner, L.R.; Leddy, J.; Zoski, C.G. *Electrochemical Methods: Fundamentals and Applications*; Wiley: New York, NY, USA, 1980.
2. Hu, X.; Li, S.; Peng, H. A comparative study of equivalent circuit models for Li-ion batteries. *J. Power Sources* **2012**, *198*, 359–367. [CrossRef]
3. Bernardi, D.; Pawlikowski, E.; Newman, J. A General Energy Balance for Battery Systems. *J. Electrochem. Soc.* **1985**, *132*, 5–12. [CrossRef]
4. Piller, S.; Perrin, M.; Jossen, A. Methods for state-of-charge determination and their applications. *J. Power Sources* **2001**, *96*, 113–120. [CrossRef]
5. Roscher, M.A.; Assfalg, J.; Bohlen, O.S. Detection of Utilizable Capacity Deterioration in Battery Systems. *IEEE Trans. Veh. Technol.* **2011**, *60*, 98–103. [CrossRef]
6. Cassani, P.A.; Williamson, S.S. Design, Testing, and Validation of a Simplified Control Scheme for a Novel Plug-In Hybrid Electric Vehicle Battery Cell Equalizer. *IEEE Trans. Ind. Electron.* **2010**, *57*, 3956–3962. [CrossRef]
7. Jossen, A. Fundamentals of battery dynamics. *J. Power Sources* **2006**, *154*, 530–538. [CrossRef]
8. Chen, M.; Rincon-Mora, G.A. Accurate electrical battery model capable of predicting runtime and I-V conductance. *IEEE Trans. Energy Convers.* **2006**, *21*, 504–511. [CrossRef]
9. Plett, G.L. Sigma-point Kalman filtering for battery management systems of LiPB-based HEV battery packs: Part 1: Introduction and state estimation. *J. Power Sources* **2006**, *161*, 1356–1368. [CrossRef]

10. Yang, J.; Du, C.; Wang, T.; Gao, Y.; Cheng, X.; Zuo, P.; Ma, Y.; Wang, J.; Yin, G.; Xie, J.; et al. Rapid Prediction of the Open-Circuit-Voltage of Lithium Ion Batteries Based on an Effective Voltage Relaxation Model. *Energies* **2018**, *11*, 3444. [CrossRef]
11. Li, Z.; Huang, J.; Liaw, B.Y.; Zhang, J. On state-of-charge determination for lithium-ion batteries. *J. Power Sources* **2017**, *348*, 281–301. [CrossRef]
12. He, Z.; Yang, G.; Lu, L. A Parameter Identification Method for Dynamics of Lithium Iron Phosphate Batteries Based on Step-Change Current Curves and Constant Current Curves. *Energies* **2016**, *9*, 444. [CrossRef]
13. Linden, D.; Reddy, T. *Handbook of Batteries*, 3rd ed.; McGraw-Hill Companies: New York, NY, USA, 2002; pp. 154–196. ISBN 0-07-135978-8.
14. Battery Test Manual for Electric Vehicles, Revision 3. Available online: https://inldigitallibrary.inl.gov/sites/STI/STI/6492291.pdf (accessed on 11 May 2019).
15. ISO 12405-1. Electrically Propelled Road Vehicles Test Specification for Lithium-ion Traction Battery Packs and Systems. Institution, British Standards, 2011. Available online: https://www.iso.org/standard/51414.html (accessed on 11 May 2019).
16. Pop, V.; Bergveld, H.J.; Danilov, D.; Regtien, P.P.; Notten, P.H. Methods for measuring and modelling a battery's electro-motive force. In *Battery Management Systems*; Springer: Dordrecht, The Netherlands, 2008.
17. Pei, L.; Wang, T.; Lu, R.; Zhu, C. Development of a voltage relaxation model for rapid open-circuit voltage prediction in lithium-ion batteries. *J. Power Sources* **2014**, *253*, 412–418. [CrossRef]
18. Pop, V.; Bergveld, H.J.; het Veld, J.O.; Regtien, P.P.; Danilov, D.; Notten, P.H.L. Modeling battery behavior for accurate state-of-charge indication. *J. Electrochem. Soc.* **2006**, *153*, A2013–A2022. [CrossRef]
19. Weng, C.; Sun, J.; Peng, H. A unified open-circuit-voltage model of lithium-ion batteries for state-of-charge estimation and state-of-health monitoring. *J. Power Sources* **2014**, *258*, 228–237. [CrossRef]
20. Ouyang, M.; Chu, Z.; Lu, L.; Li, J.; Han, X.; Feng, X.; Liu, G. Low temperature aging mechanism identification and lithium deposition in a large format lithium iron phosphate battery for different charge profiles. *J. Power Sources* **2015**, *286*, 309–320. [CrossRef]
21. Lu, L.; Han, X.; Li, J.; Hua, J.; Ouyang, M. A review on the key issues for lithium-ion battery management in electric vehicles. *J. Power Sources* **2013**, *226*, 272–288. [CrossRef]
22. Introduction of BMS Products. Available online: http://www.hyperstrong.net/bms.html (accessed on 20 December 2018).
23. Chen, Y.; Liu, X.; Yang, G.; Geng, H. An Internal Resistance Estimation Method of Lithium-ion Batteries with Constant Current Tests Considering Thermal Effect. In Proceedings of the IECON 2017 -43rd Annual Conference of the IEEE Industrial Electronics Society, Beijing, China, 29 October–1 November 2017.
24. Waag, W.; Käbitz, S.; Sauer, D.U. Experimental investigation of the lithium-ion battery impedance characteristic at various conditions and aging states and its influence on the application. *Appl. Energy* **2013**, *102*, 885–897. [CrossRef]
25. Pattipati, B.; Balasingam, B.; Avvari, G.V.; Pattipati, K.R.; Bar-Shalom, Y. Open circuit voltage characterization of lithium-ion batteries. *J. Power Sources* **2014**, *269*, 317–333. [CrossRef]